Photovoltaic-System Participation in Power-System Frequency Response under High Renewable Energy Penetration

CHIEN-KUO CHANG
Department of Electrical Engineering
National Taiwan University of Science and Technology

YU-CHI LIU
Department of Electrical Engineering
National Taiwan University of Science and Technology

HUA-WEN TSAI
Department of Electrical and Information Technology
Nankai University of Science and Technology

FU-YEN LIN
Department of Electrical Engineering
National Taiwan University of Science and Technology

National Taiwan University of Science and Technology, Taipei, Taiwan (R.O.C.)
Nankai University of Science and Technology, Nantou, Taiwan (R.O.C.)

Corresponding author: chienkuo@mail.ntust.edu.tw

Abstract: - The increasing penetration of power-electronics–based renewable energy has reduced the electric-system inertia and operating reserve, leading to concerns about the frequency stability of power systems. This study explores the participation of photovoltaic sources in the frequency-response regulation of power systems through the deloading process and analyzes relevant scenarios to investigate the effects of varying penetration levels of renewable energy and deload margins on the frequency response of the power system. To observe the performance of the system in different scenarios, simulations are performed based on the IEEE 39-bus system with renewable-energy penetration levels of 0–50% and deload margins of 0–50%. The selection method for suitable deload margin was presented according to frequency response and generation lost.

Key-Words: - Renewable energy, inertia response, frequency response, deloading, renewable penetration
Received: July 25, 2023. Revised: March 2, 2024. Accepted: April 13, 2024. Published: May 22, 2024.

1. Introduction

In response to climate change, countries around the globe have been advocating the adoption of renewable energy sources to improve the environment and energy security [1]. Major countries have formulated relevant measures and regulations to promote renewable-energy development. For example, the US passed the Inflation Reduction Act of 2022 and the European Union passed the REPowerEU plan.

However, the increasing of renewable energy probably affects the stability of power systems. Research has shown that the integration of energy storage systems (ESSs) is a possible solution to address these challenges. The grid stability can also be improved by adjusting the devices used for renewable-energy generation [2]. The use of an ESS to provide virtual inertia and avoid frequency violations during contingency periods has also been proposed recently [3][4].

Although the ESS assists in improving the resilience of power systems in high-penetration-ratio situations, the cost of investment can be a problem during deployment. Hence, a power-reserve-control tracking algorithm based on the curtailed power–current curve has been proposed [5][6]. Forecasting-based virtual inertia control and coordinated reserve strategies have also been developed [7]. The frequency response of renewable sources is required in grid codes to ensure stable and regular operation [8][9]. The German grid code requires renewable energy sources to provide frequency support to the power grid [10].

The frequency support provided by photovoltaic (PV) and wind sources, for frequencies less than the nominal frequency, which decreases the output, is called the deload method. Reference [11] proposed a deloaded operation for large-scale PV power plants and a fast frequency response that promptly supported system-frequency recovery after major contingencies. The implementation of deloading in PV equipment can facilitate dynamic control of the PV power reserve through reserve power point tracking [12][13]. The average PV power output can be adjusted dynamically by periodically activating and deactivating the maximum power point (MPP). This can secure reserve power for greater grid stability and reliability. Reference [14] proposed a method for determining the optimal deloading size by considering both economic factors and frequency stability.

This study focuses on the stability of a power system by simulating fault events in an electric grid. Various penetration levels of renewable energy, from 0 to 50%, are simulated. Subsequently, the improvement in stability is discussed using the deload function embedded in the PV model. This study is expected to be beneficial while planning the energy policy when the renewable instant penetration rate approaches high levels (exceeding 40%).

The remainder of this paper is organized as follows: an overview of renewable energy and the approaches for deloading systems are provided in Section 2. In Section 3, the participation of PV systems in frequency regulation is introduced. The deloading scenarios for deloaded systems are presented in Section 4. In Section 5, the simulations using the IEEE 39-bus system are described, and Section 6 presents the conclusions of this work.

2. Renewable energy and approaches for deloading systems

The stability of a power system relies primarily on synchronous generators, which are synchronized to the frequency of the grid and store kinetic energy via rotational mechanics. In the face of an imbalance between the power supply and demand, these generators can automatically adjust their rotational speed and release the stored kinetic energy, converting it into electrical power to maintain balance.

With its increasing adoption, renewable energy is expected to be the primary source of power generation in the future power grids. However, the interface between the renewable energy sources and grid often uses power-electronic devices, which facilitate the decoupling of renewable-energy generation systems from the grid, leading to a reduction in the inertia of the entire system.

With less rotational inertia directly connected to the grid, an alternative to improve the system inertia is necessary. Therefore, methods have been developed to simulate system inertia and enable renewable energy sources to actively participate in frequency-response control. The following sections introduce the frequency-support methods for wind- and PV-based power-generation systems.

2.1 Wind turbines

Currently, wind-power generation relies primarily on three control techniques to facilitate frequency response: inertia response, droop, and deloading control. Inertia-response control allows wind turbines to effectively release the kinetic energy stored within their rotating blades, thereby reducing frequency deviations. Droop control adjusts the power output in response to frequency variations. Deloading control adjusts the blade angles and rotation speeds of the wind turbine to provide a certain power reserve to satisfy unexpected imbalances between power generation and demand.

For economic reasons, wind turbines are typically operated at the MPP, without additional power reserves that participate in frequency control. The deloading process shifts the operating point of a wind turbine from the MPP to a lower point, to allocate the reserve power [15][16]. The performance of a wind turbine varies according to the blade angle. By increasing the blade angle, the operating point can be reduced from the MPP to the deloading point while maintaining a constant rotational speed.

2.2 Photovoltaic system

PV power plants typically operate at their MPPs to achieve optimal efficiency. By employing deloading control, the system can participate in the frequency-response control with a power reserve. The operating point can be adjusted by increasing or decreasing the voltage. Conventionally, voltage levels are raised beyond the MPP to obtain the desired operating point for a deloaded system [17].

Fig. 1 illustrates the deloading process and its control strategies. As can be observed from the figure, the reference voltage is related to the MPP (V_{MPP}), deloading voltage (V_{deload}), and frequency variation (Δf).

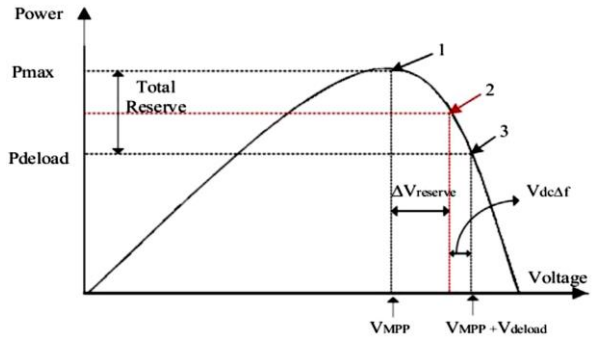

Fig. 1. Diagram of deloading control [17].

Equation (1) shows that the generator initially operates at MPP "1", with an operating voltage of V_{MPP}. By introducing an additional voltage (denoted as V_{deload}), the operating point of the generator is shifted to a lower point "3". The power reserve is defined as the difference between the maximum power (P_{max}) and deloaded power (P_{deload}).

$$V_{\mathrm{dc,ref}} = V_{\mathrm{MPP}} + V_{\mathrm{deload}} - V_{\mathrm{dc,\Delta f}} \ldots\ldots \quad (1)$$

3. Participation of PV system in frequency regulation

In this study, the frequency response from the PV system was simulated using the PSS®E software. A generic model of a PV system was used following the guidelines provided by the Western Electricity Coordinating Council (WECC). In simulations, a PV system should be represented by a single generator with an equivalent power capacity; therefore, all the PV power plants considered in this study were represented by their equivalent generators.

The generic WECC PV model comprises three renewable energy dynamic models: Renewable Energy Plant Controller_A (REPC_A), Renewable Energy Electrical Controls Model_B (REEC_B), and Renewable Energy Generator/Converter Model_A (REGC_A). These models can be used to simulate the transient responses of PV systems. PSS®E was used for both steady-state power-flow calculations and dynamic-response simulations. As mentioned earlier, the deloading control reduced the PV output power from its MPP (P_{mpp}) to a target deloaded point (P_{deload}). Therefore, the steady-state power output was reduced in the simulations to produce a power reserve. For the dynamic simulations, the power output of the PV system was adjusted according to system-frequency variations.

3.1 Settings of dynamic simulations

The frequency response of the PV system was mainly obtained through the frequency control of the renewable energy power converter (REPC) module. Fig.2 illustrates the frequency-control process. The frequency variation was determined based on the deadband (DB). If the input was within a predefined range, no observable response existed. However, if the input exceeded the DB threshold, the control system applied a predetermined gain specified in the droop control to the frequency variation, resulting in a varying power output.

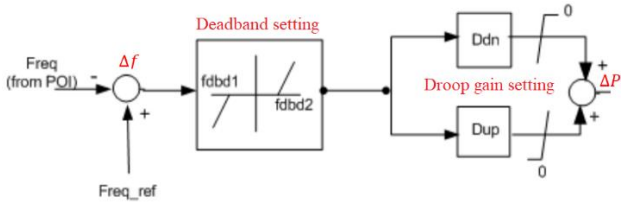

Fig. 2. Schematic of frequency control in the REPC module.

In this study, the power reserve was produced by the deloaded PV system, and was similar to the inertial response from synchronous generators. Therefore, the DB was not predetermined, to allow prompt power compensation for the PV system. Droop control involves a lower droop gain (D_{dn}) for over-frequency protection and a higher droop gain (D_{up}) for under-frequency protection. Our model simulated the frequency decline following a neutral to ground (N–G) voltage problem; therefore, $\mathrm{D_{up}}$ was used. The operating curve was set based on the Taipower Regulation Reserve "dReg0.5", wherein PV systems were required to deliver full power output when the system frequency decreased below 59.5 Hz.

As shown in Fig. 2, the output variation of the REPC module is: $\Delta P = \Delta f \times D_{\text{up}}$. D_{up} can be obtained using Equations (2)–(4): In (2), ΔP represents the power variation, which is the difference between the MPP (P_{mpp}) and deloaded power (P_{deload}). In (3), Δf denotes the frequency deviation, which is the per-unit value of the difference between the utility frequency (60 Hz) and predetermined full-load output frequency (59.5 Hz). The slope can then be obtained using (4).

$$\Delta P = P_{mpp} - P_{deload} \text{ p. u.} \quad \text{..... (2)}$$

$$\Delta f = \frac{60-59.5}{60} = 0.00833 \text{ p. u.} \quad \text{..... (3)}$$

$$D_{\text{up}} = \frac{\Delta P}{\Delta f} = \frac{P_{mpp}-P_{deload}}{0.00833} \quad \text{..... (4)}$$

A power–frequency response curve of the PV system can then be obtained, as shown in Fig.3. The right half of the curve shows that, when the frequency exceeds the nominal value (60 Hz), the maximum output is curtailed under the deload value. As the frequency decreases, the PV system adapts its output power according to the slope (D_{up}) until a predetermined upper power limit is attained.

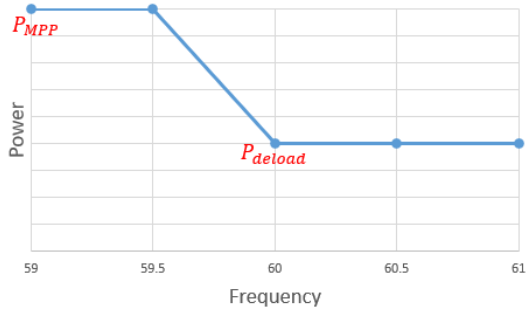

Fig. 3. Power–frequency response curve.

3.2 Model validation

The effectiveness of the frequency regulation in the PV system was verified using a simplified model consisting of a PV unit and two traditional generators (G1 and G2), as illustrated in Fig. 4. At the 2nd second, G2 was tripped to observe whether the variations in the frequency and PV output conformed to the predefined settings. Both G1 and G2 were modeled using the PSS®E model GENSAE for salient-pole generators. In the modeling of the governor, the DEGOV diesel governor model was used and the rate of change of speed was set to 0.05.

The maximum power of the PV system was set to 0.4 p.u., which was subsequently reduced to 0.35 p.u. for deloading control. According to (3), the droop gain D_{up} =6. Fig. 5 and 6 show the variations in the frequency and output power, respectively, after the fault.

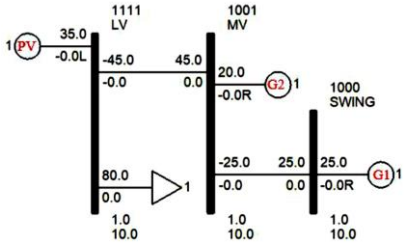

Fig. 4. Model used for testing.

According to the frequency-variation curve, the maximum frequency variation was -0.0073 p.u. with a steady-state frequency deviation of -0.0049 p.u. By substituting these values in $\Delta P = \Delta f \times D_{\text{up}}$, the maximum variation in power was obtained as 0.0438 p.u., with a steady-state deviation of 0.0294 p.u. By adding these two values to the initial power (0.35 p.u.), the maximum post-fault output power (0.3938 p.u.) and steady-state output power (0.3794 p.u.) were determined. These calculated values were in line with the PSS®E simulated results, suggesting the effectiveness of frequency control with the proposed model.

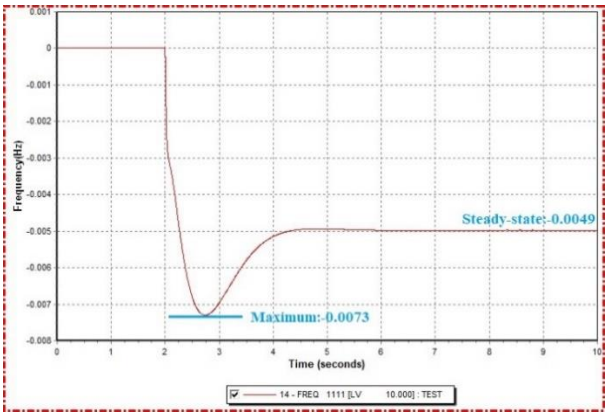

Fig. 5. Frequency deviation.

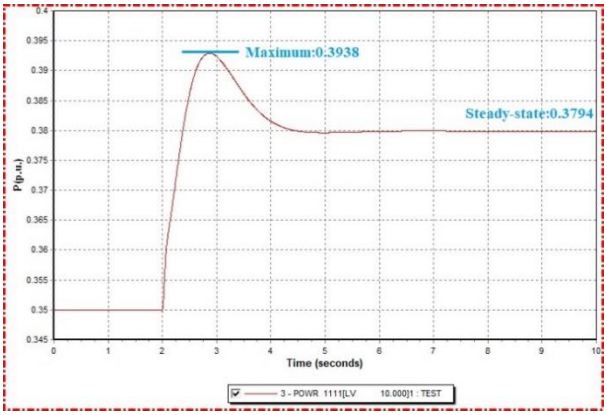

Fig. 6. PV output variation.

4. Deloaded scenarios

The deloaded PV system in this study was based on the IEEE 39-bus system, which is a power network in the New England area of the US, with 10 generators, 39 busbars, 12 transformers, and 19 loads. To simulate the frequency response of the PV system, 6 additional PV units were introduced into the model at buses 13, 15, 23, 26, 27, and 28, as shown in Fig. 7. The generation of the PV units was set to the same average as the total renewable penetration. Simulations were performed for different PV scenarios with varying PV penetration levels and deload margins. The simulation results were organized and analyzed to investigate the influences of the parameters on the frequency response of the system.

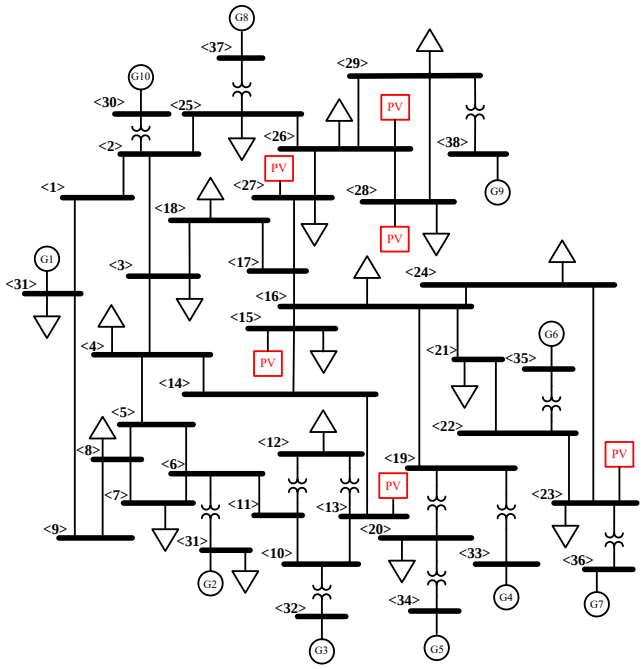

Fig. 7. The IEEE 39-bus system and the additional PV units.

The penetration level of renewable energy is defined as the ratio of renewable energy generated to the total power generated. In this study, the PV penetration level was calculated as the proportion of PV output to the total output, in range of 10–50%. To maintain the total generation capacity of the original system at 5,913 MW, the power output of the PV system was incrementally increased while reducing the output of the traditional generators. At each penetration level, six scenarios (deload margins from 0% to 50%) were simulated to explore the effect of deloading control on the frequency response. The configuration of energy sources for each scenario is listed in Table 1.

The simulation of each scenario lasted 10 s. The system was operated under normal conditions for the first two seconds. At the 2nd second, two generators (G6 on Bus 35 and G9 on Bus 38) were tripped to observe the swing in the bus, if any. The two generators were tripped to set the frequency to the lower limit (59.5 Hz) after the fault event.

Table 1. Simulation scenarios

	PV penetration level (MW)	Power output of conventional generators (MW)	Power output of PV systems (MW)	Deload margin (%)
Original system	0%	5,913	0	
PV system	10%	5,322	591	0, 10, 20, 30, 40, 50
	20%	4,731	1,182	
	30%	4,139	1,774	
	40%	3,549	2,364	
	50%	2,955	2,958	

4.1 Effect of deloaded PV system

Two simulation methods were employed to test the effectiveness of the deloading control in improving the frequency response. Both methods used a PV penetration level of 50% as the reference.

The first method involved redistribution of the deloaded power to the target units, to generate the same power as the traditional generators across three scenarios (without deloading control, 10% deload margin, and 20% deload margin). Consequently, the steady-state frequency remained unchanged for these three scenarios, allowing direct observation of the positive effect of the deloaded PV system on the frequency response. However, such an effect varied owing to varying fault conditions, and the decline in frequency in the early fault stage differed accordingly.

As shown in Fig. 8, the frequency decline increased with an increase in the deload margin. Notably, the most substantial decline was observed in the blue curve (20% deload margin), which was primarily attributed to the highest power generation capacity, in this specific case. However, under the same steady-state frequency conditions, the deloaded PV system allowed a greater tripped capacity than the PV system without deloading control. Furthermore, the results revealed that the deloaded PV system recovered more rapidly after reaching the minimum frequency point.

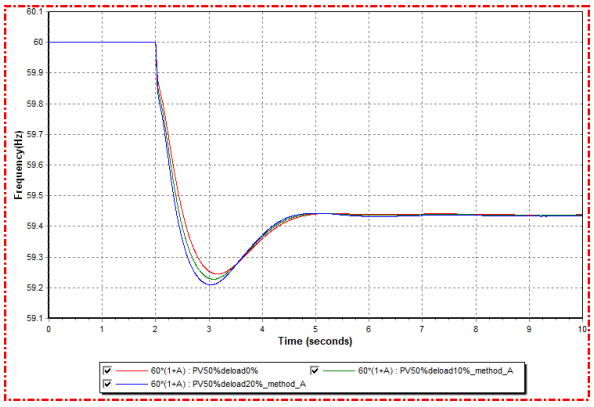

Fig. 8. Total tripped capacities of the fire generators are different, but the total generations of the existing fire units are the same.

Although the first method is useful for maintaining a steady-state frequency, its effect differs according to the varying generation drop. The second method provides power compensation by reducing the load on the deloaded PV system. Using this method, the fault has the same impact on the system, without affecting the generation drop. However, the steady-state frequency differs according to the variations in the power supply and demand after the steady state.

Fig. 9 shows the frequency-response curves for scenarios with 20% deload margin (blue), 10% deload margin (green), and without deloading control (red). As can be observed, an increase in the deload margin reduces the extent of frequency decline and produces a corresponding elevation in the minimum frequency, suggesting the effectiveness of deloading control in improving the frequency response.

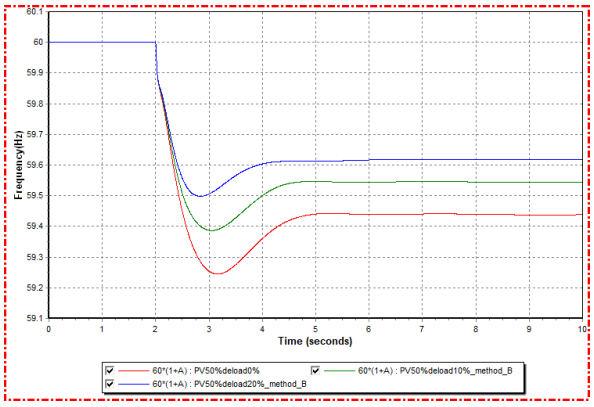

Fig. 9. Total tripped capacities of the fire generators are the same, but the total generations from the existing fire units are different.

The above simulation results indicate that the deloaded PV system can be used to enhance the frequency response. In the subsequent simulations, the reduction in the output power of the PV system is compensated by the traditional generators. In other words, the outputs of the traditional generators differ for different scenarios. This approach offers a closer representation of real-world scenarios in which fluctuations in PV power generation are mitigated by adjusting the outputs of the traditional generating units.

4.2 Frequency-response indices

To visualize the results, three indices were used to quantify the frequency response: rate of change of frequency (RoCoF), lowest frequency point (f_{nadir}), and steady-state frequency ($f_{steady\ state}$). The RoCoF refers to the speed at which the frequency changes. It is calculated as the time derivative of the frequency from the start of the fault until the lowest point. The lowest frequency point is the frequency at the valley of the frequency-response curve.

$$RoCoF(Hz/sec.) = \frac{df}{dt} = \frac{\Delta f_{MAX}}{t_{fault} - t_{nadir}} \ldots \quad (5)$$

Simulations were performed to compare the effects of PV systems with different PV penetration levels on the frequency response in three deloading scenarios (without deloading control, 10% deload margin, and 20% deload margin).

5. Simulation of the IEEE 39-bus system

Modeling was conducted based on the IEEE 39-bus system with six additional PV units. Simulations were conducted for different PV scenarios with various PV penetration levels and deload margins. This section first discusses the influence of the PV penetration level on the frequency response, and then explores the combined impact of PV penetration and deloading control on the frequency response of the power system.

5.1 PV penetration levels

Fig. 10 shows a comparison of the frequency responses at different PV penetration levels without deloading control. Each curve in the figure corresponds to a PV penetration level: from the top to the bottom, they are: red (original system), green (10%), yellow (20%), blue (30%), gray (40%), and pink (50%). As shown in the left half of the figure, the frequency decreases rapidly, from the red curve at the top to the pink curve at the bottom, with a gradual increase in the PV penetration level.

The lowest frequency is attained quickly, and the

minimum frequency is lower. This is mainly attributed to the decline in the overall system inertia caused by an increase in the PV penetration level. Consequently, the frequency response is poor in the early fault stage, and the frequency decreases rapidly. The right half of the figure shows the motion of the governor, which is not affected by the system inertia. Therefore, after the frequency recovery, the steady-state frequency of the original system remains at the highest point (red curve), whereas that of the system with the highest PV penetration level (pink curve) is the lowest.

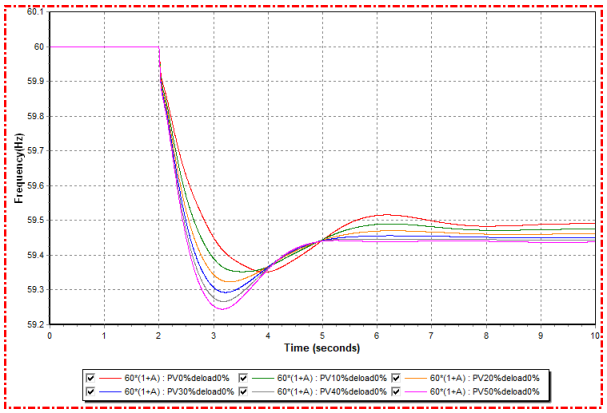

Fig. 10. Frequency responses at various PV penetration levels (without deloading control).

Table 2 summarizes the frequency-response indices of PV systems without deloading control. As the PV penetration level increases, the RoCoF increases from an initial value of -0.3353 Hz/s to -0.6535 Hz/s (a difference of 0.32 Hz/s). Moreover, the lowest frequency increases with higher PV penetration levels. For instance, in the original system, the lowest frequency was attained at 3.935 s, whereas in the system with a PV penetration level of 50%, the lowest frequency is attained at 3.156 s, which is approximately 0.8 s earlier. This implies that the system has less time to respond. Both the lowest and steady-state frequencies decrease slightly as the PV penetration level increases. However, the change is not significant, with both values being approximately 0.1 Hz.

The above indicators show that the frequency response of the power system degrades as the PV penetration level increases, which is mainly affected by the system inertia. In the early fault stage, the RoCoF increased significantly with increasing PV penetration, and the system attained the lowest frequency quickly. Consequently, the system had to respond to changes within a short time. However, the existing frequency-protection measures of the system may not be adequate for effectively addressing new fault scenarios. Therefore, additional attention should be given to these situations.

Table 2. Indices for PV system without deloading

PV penetration level	RoCoF (Hz/s)	f_{nadir} (Hz)	t_{nadir} (s)	$f_{steady\ state}$ (Hz)
0%	-0.335	59.35	3.935	59.49
10%	-0.426	59.35	3.519	59.47
20%	-0.527	59.32	3.286	59.46
30%	-0.578	59.29	3.223	59.45
40%	-0.622	59.27	3.179	59.44
50%	-0.654	59.24	3.156	59.44

5.2 Deloading control in PV systems

This subsection introduces the simulations for scenarios with various PV penetration levels and deload margins, and presents the relevant indices. 0 shows the frequency-response curves for PV systems with a deload margin of 20% and different penetration levels of 10% (red), 20% (green), 30% (yellow), 40% (blue), and 50% (grey). Compared to the scenarios without deloading, presented in Fig. 11, the five curves exhibit considerable differences when the deload margin is 20%. The variations among the curves, in terms of the steady-state frequency, minimum frequency, and time at which the minimum frequency is attained, become more pronounced.

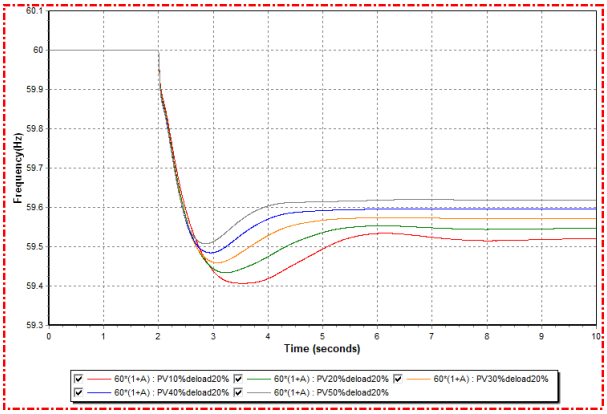

Fig. 11. Frequency responses at various PV penetration levels (with a 20% deload margin).

Table 3 lists the frequency-response indicators for PV systems with a deload margin of 20% and different penetration levels. As can be observed from the table, as the penetration level increases, the variations in all indicators become greater than that observed with a deload margin of 10%. The difference in the lowest frequencies for penetration levels of 10% (59.41 Hz) and 50% (59.51 Hz) is approximately 0.1 Hz, which remains consistent

across all penetration levels with a deload margin of 20%. However, the maximum variation is observed in the steady-state frequency, which is 0.1 Hz and twice the frequency in scenarios with a 10% deload margin (0.05 Hz).

Table 3. Indices for a system with 20% deload margin

Penetration level	RoCoF (Hz/s)	f_{nadir} (Hz)	t_{nadir} (s)	$f_{steady\ stat}$ (Hz)
10%	-0.3854	59.41	3.539	59.52
20%	-0.4645	59.43	3.219	59.55
30%	-0.5010	59.46	3.079	59.57
40%	-0.5409	59.48	2.953	59.60
50%	-0.5752	59.51	2.856	59.62

Fig. 12 shows the frequency-response curves of PV systems with a deload margin of 50% for different penetration levels. Compared to the scenarios with a deload margin of 20%, the five curves are all raised because of more reserved power.

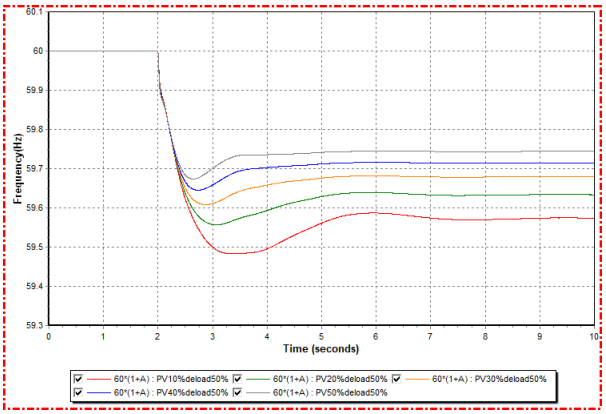

Fig. 12. Frequency responses at various PV penetration levels (with a 50% deload margin).

Table 4 lists the frequency-response indicators. The difference in the lowest frequency at penetration levels of 10% (59.48 Hz) and 50% (59.67 Hz) is approximately 0.19 Hz. In addition, the steady-state frequencies are 59.57 Hz for the 10% penetration level and 59.74 Hz for the 50% penetration level.

Table 4. Indices for a system with 50% deload margin

Penetration level	RoCoF (Hz/s)	f_{nadir} (Hz)	t_{nadir} (s)	f_{ss} (Hz)
10%	-0.379	59.48	3.36	59.57
20%	-0.417	59.56	3.06	59.63
30%	-0.449	59.61	2.87	59.68
40%	-0.489	59.65	2.73	59.72
50%	-0.510	59.67	2.64	59.74

The RoCoF, which is the most important transient indicator, and the relationship between the PV deload margin and renewable penetration level are shown in Fig. 13. The criterion of RoCoF is -0.5 Hz/s, as indicated by the dashed red line. There are six groups of PV deload margins: 0, 10, 20, 30, 40, and 50%, with each group consisting of five renewable penetration levels from 10 to 50%.

In each group, the RoCoF decreases with increase in the renewable energy penetration level; hence, the grid weakens. Among the six groups, the RoCoF decreases with increasing PV deload margin, such that the grid becomes resilient. For a 0% PV deload margin, the maximum renewable penetration is lower than 20% without an RoCoF that is lower than threshold. If the maximum renewable penetration is set to be 30 or 40%, the PV deload margin should be greater than 20 or 50%, respectively.

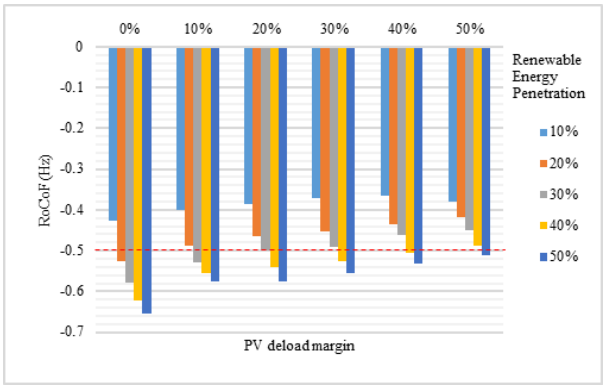

Fig. 13. Relationship of RoCoF between PV penetration level and deload margin.

Fig. 14 shows the relationship between the deload margin and renewable penetration level. f_{nadir} should be 59.5 Hz, as indicated by the dashed red line. A higher f_{nadir} value represents better reliability of the power grid. For a 0% PV deload margin, f_{nadir} reduces while the renewable energy penetration increases. However, the problem of deploying renewable energy is evident.

The impact of increasing renewable energy penetration is positive when the deload margin is greater than 20%. In contrast, f_{nadir} increases as the renewable energy penetration increases. It is apparent that the deload method can improve the resilience of the power grid with high penetration.

These findings suggest that, at the same penetration level, a higher deload margin leads to a better frequency response. In other words, the greater the power reserve of the PV system, the greater the improvement in its frequency response.

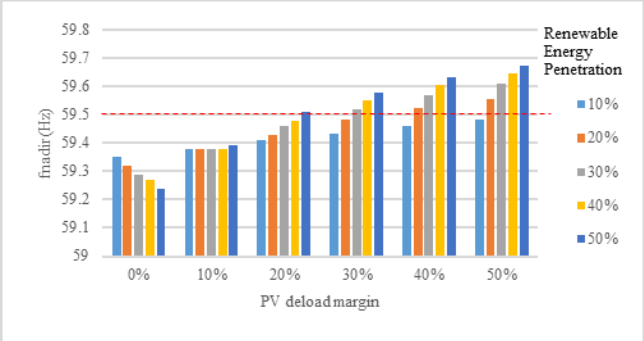

Fig. 14. Relationship of f_{nadir} between PV penetration level and deload margin.

6. Discussion

The system responses were compared in scenarios without deloading control and with a deload margin of 20%, for different penetration levels. In scenarios without deloading control, the increase in PV penetration clearly affected the overall inertia of the system. As the penetration level increased, the system responded poorly in the early fault stage, raising concerns regarding the adequacy of existing protective measures to effectively address fault scenarios under higher penetration levels. In scenarios with 20% deload margin, higher penetration levels led to better frequency responses, owing to the increased power reserve from the PV system. With more power reserves, the system responded better to contingencies, resulting in a better frequency response.

In practice, the PV deload will curtail the generation of PV energy such that the income of the company is reduced. Hence, understanding the relationship between the frequency reserve and curtailed energy is key. Fig. 15 shows the generation curves for different PV deload margins, based on normally distributed sunlight. The deload function curtails energy around the peak time. However, the banded generation is not proportional to the deload margin. For example, the banded generation with 50% deload margin is less than 50% of the generated energy without deload.

Fig. 16 shows the relationships for PV deload margins from 0 to 100%. The generated energy decreases as the PV margin increases, as indicated by the blue and orange lines. These two lines intersect at a deload margin of approximately 60–70%. The suitable deload margin can be lower than that in the intersection region because the wasted generation exceeds half of the total energy, without curtailment.

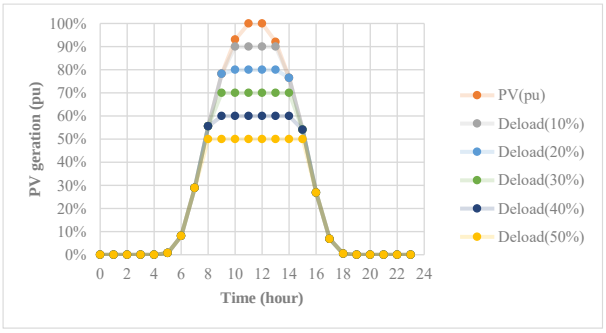

Fig. 15. Generation curves for different PV deload margins.

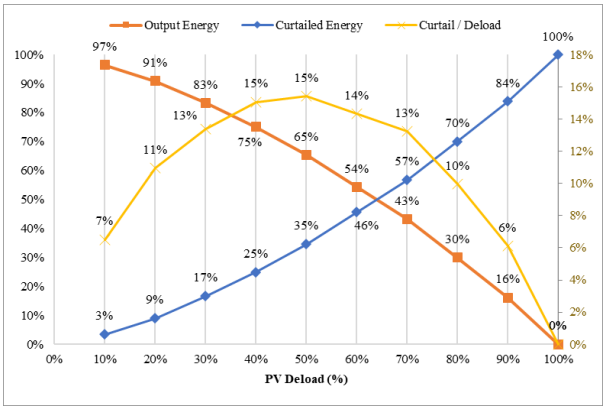

Fig. 16. Relationships for PV deload margins from 0 to 100%.

The ratio of the curtailed energy to the deload margin, represented by the yellow line, indicates the effectiveness of the deloading control. The higher this ratio, the higher the curtailed energy for the same deloading capacity. Hence, a suitable deload margin should be around the peak region of 40–50%.

Considering these conditions, the deload margin suggested in this study is approximately 40%, which retains 75% of the generation, wasting only 25%. According to Fig. 15, it is not necessary to perform PV deloading continuously; an appropriate operating time would be between 9 and 14, totaling six hours.

7. Conclusion

In this study, a model was built based on the IEEE 39-bus system to simulate the frequency responses related to the deloading control for PV systems with different renewable energy penetration levels. The trade-off between the frequency response and lost energy was discussed. A suitable deload margin (approximately 30–50%) was suggested, with an optimal value of 40% for this study.

Although the simulated power grid in this study was small and a solitary case, the proposed method

can be utilized in any real scenario. The benefit of the deload method realized for PV and wind power is that it reduces the use of expensive ESSs. The optimization involving the use of both renewable deloading and ESS should be further studied.

References

[1] International Energy Agency, "Electricity market report 2023," February 2023

[2] K N. Akpinar, B. Gundogdu, O. Ozgonenel and C. Gezegin, An Intelligent Power Management Controller for Grid-connected Battery Energy Storage Systems for Frequency Response Service: A Battery Cycle Life Approach, *Electric Power Systems Research*, Vol. 216, 2023.

[3] U. Datta, A. Kalam and J. Shi, Battery Energy Storage System Control for Mitigating PV Penetration Impact on Primary Frequency Control and State-of-Charge Recovery, *IEEE Transactions on Sustainable Energy*, Vol.11, No.2, 2020, pp. 746-757.

[4] R. Aljarrah, B. B. Fawaz, Q. Salem, M. Karimi, H. Marzooghi and R. Azizipanah-Abarghooee, Issues and Challenges of Grid-Following Converters Interfacing Renewable Energy Sources in Low Inertia Systems: A Review," *IEEE Access*, Vol.12, 2024, pp. 5534-5561.

[5] A. F. Hoke, M. Shirazi, S. Chakraborty, E. Muljadi and D. Maksimovic, Rapid Active Power Control of Photovoltaic Systems for Grid Frequency Support, *IEEE Journal of Emerging and Selected Topics in Power Electronics*, Vol.5, No.3, 2017, pp. 1154-1163.

[6] C. Zhong, Y. Zhou and G. Yan, A Novel Frequency Regulation Strategy for a PV System Based on the Curtailment Power-Current Curve Tracking Algorithm, *IEEE Access*, Vol.8, 2020, pp. 77701-77715.

[7] J. Chang, Y. Du, E. G. Lim, H. Wen, X. Li and L. Jiang, Coordinated Frequency Regulation Using Solar Forecasting Based Virtual Inertia Control for Islanded Microgrids, *IEEE Transactions on Sustainable Energy*, Vol.12, No.4, 2021, pp. 2393-2403.

[8] M. T. Hagh and T. Khalili, A Review of Fault Ride through PV and Wind Renewable Energies in Grid Codes, *International Journal of Energy Research*, Vol.43, 2019, pp. 1342-1356.

[9] E. Serban, M. Ordonez and C. Pondiche, Voltage and Frequency Grid Support Strategies beyond Standards, *IEEE Transactions on Power Electronics*, Vol.32, No.1, 2017, pp. 298-309.

[10] T. D. Reddy, J. R. Dash and P. Agarwal, A New Control Strategy of a Single Stage PV System for Providing Frequency Support to the Power Grid," *2023 IEEE IAS Global Conference on Emerging Technologies (GlobConET)*, London, United Kingdom, pp. 1-5, 2023.

[11] C. Rahmann and A. Castillo, "Fast Frequency Response Capability of Photovoltaic Power Plants: The Necessity of New Grid Requirements and Definitions, *Energies* 2014, Vol.7, pp. 6306-6322.

[12] A. Narang, H. D. Tafti, J. Pou and G. Konstantinou, Dynamic Reserve Power Point Tracking in Grid-Connected Photovoltaic Power Plants, *IEEE Transactions on Power Electronics*, Vol.38, 2023, pp. 5939-5951.

[13] E. I. Batzelis, G. E. Kampitsis and S. A. Papathanassiou, Power Reserves Control for PV Systems With Real-Time MPP Estimation via Curve Fitting, *IEEE Transactions on Sustainable Energy*, Vol.8, No.3, 2017, pp. 1269-1280.

[14] I. Mahmud, N.-A. Masood and Atik Jawad, Optimal Deloading of PV Power Plants for Frequency Control: A Techno-Economic Assessment, *Electric Power Systems Research*, Vol.221, 2023.

[15] K. V. Vidyanandan and N. Senroy, Primary Frequency Regulation by Deloaded Wind Turbines using Variable Droop, *IEEE Transactions on Power Systems*, Vol.28, 2013, pp. 837-846.

[16] L. M. Castro, C. R. Fuerte-Esquivel and J. H. Tovar-Hernández, Solution of Power Flow with Automatic Load-Frequency Control Devices including Wind Farms, *IEEE Transactions on Power Systems*, Vol.27, 2012, pp. 2186-2195.

[17] M. Dreidy, H. Mokhlis and S. Mekhilef, Inertia Response and Frequency Control Techniques for Renewable Energy Sources: A Review, *Renewable Sustainable Energy Reviews*, Vol.69, 2017, pp. 144-155.